metals

MDPI

Article

Study on Nitrogen-Doped Biomass Carbon-Based Composite Cobalt Selenide Heterojunction and Its Electrocatalytic Performance

Tengfei Meng [1], Hongjin Shi [1], Feng Ao [1], Peng Wang [1], Longyao Wang [1], Lan Wang [1], Yujun Zhu [2], Yunxiang Lu [3] and Yupei Zhao [1,*]

[1] School of Petrochemical Engineering, Changzhou University, Changzhou 212006, China
[2] Department of Pharmaceutical and Biomedical Engineering, Clinical College of Anhui Medical University, Hefei 230031, China
[3] School of Chemical and Molecular Engineering, East China University of Science and Technology, Shanghai 200237, China
* Correspondence: zhaoyupei@cczu.edu.cn

Abstract: With the increasing utilization of clean energy, the development and utilization of hydrogen energy has become a research topic of great significance. Cobalt selenide (CS) is an electrocatalyst with great potential for oxygen evolution reaction (OER). In this paper, a nitrogen-doped biomass carbon (1NC@3)-based composite cobalt selenide (CS) heterojunction was prepared via a solvothermal method using kelp as the raw material. Structural, morphological, and electrochemical analyses were conducted to evaluate its performance. The electrochemical test results demonstrate that the overpotential of the CS/1NC@3 catalyst in the OER process was 292 mV, with a Tafel slope of 98.71 $mV \cdot dec^{-1}$ at a current density of 10 $mA \cdot cm^{-2}$. The electrochemical performance of the CS/1NC@3 catalyst was further confirmed by theoretical calculations, which revealed that the presence of the biomass carbon substrate enhanced the charge transport speed of the OER process and promoted the OER process. This study provides a promising strategy for the development of efficient electrocatalysts for OER applications.

Keywords: cobalt selenide; electrocatalysis; biomass; DFT

check for updates

Citation: Meng, T.; Shi, H.; Ao, F.; Wang, P.; Wang, L.; Wang, L.; Zhu, Y.; Lu, Y.; Zhao, Y. Study on Nitrogen-Doped Biomass Carbon-Based Composite Cobalt Selenide Heterojunction and Its Electrocatalytic Performance. *Metals* **2023**, *13*, 767. https://doi.org/10.3390/met13040767

Academic Editor: Thomas Gries

Received: 4 March 2023
Revised: 26 March 2023
Accepted: 11 April 2023
Published: 14 April 2023

Copyright: © 2023 by the authors. Licensee MDPI, Basel, Switzerland. This article is an open access article distributed under the terms and conditions of the Creative Commons Attribution (CC BY) license (https://creativecommons.org/licenses/by/4.0/).

1. Introduction

Traditional energy has brought severe environmental issues, and the depletion of non-renewable resources has prompted humans to develop and research new energy sources [1]. Hydrogen energy is an ideal clean energy source, and water electrolysis is an ideal process for producing hydrogen. Oxygen Evolution Reaction (OER), which takes place at the anode, is the rate-determining step of water electrolysis for hydrogen production and has become an area of extensive research [2–4]. Platinum (Pt) and its alloys have always been considered excellent electrocatalysts; however, their high cost and low durability significantly impede their commercial application. Biomass energy is an important energy source for human survival; thus, it is of great research significance to use biomass to replace non-renewable resources. The combination of the electrode material prepared from biomass as the carbon source with hydrogen energy is currently a research hotspot [5–7].

As a renewable resource, algae are widely found in oceans and lakes. Elements such as nitrogen, phosphorus, calcium, and iron are evenly distributed in biomass, which can be synthesized in situ into self-doped carbon materials after being carbonized without having to add additional heteroatom dopants [8]. The uniform distribution of elements can improve carrier mobility, thereby effectively improving the material's electrochemical performance. Pérez-Salcedo, K.Y et al. used Sargassum as a carbon source, activated it with potassium hydroxide, and then doped it with hydrazine sulfate to obtain a catalyst with a

surface area of 2289 $m^2 \cdot g^{-1}$, a nitrogen content of 0.16%, and a sulfur content of 2.63%. This showed good ORR activity [9]. Wang, F. et al. developed a self-doping electrocatalyst from rice husk biomass, where the self-doping of Si in the rice husk biomass improved the degree of graphitization of the catalyst. The prepared catalyst had good electrocatalytic activity, good stability (a retention rate greater than 85% after 40,000 s), and methanol tolerance [10]. Hao et al. used seaweed biomass sodium alginate to prepare defective carbon catalysts with good ORR activity and selectivity comparable to commercial Pt/C catalysts. The catalysts exhibited better stability and methanol tolerance than Pt/C catalysts [11]. It is clear that the research and development of biomaterials as electrocatalysts have the potential to replace noble metal catalysts.

Previous studies have shown that OER electrocatalysts based on transition metals typically demonstrate high over-potentials [12]. However, cobalt-based materials, including CoS_2 [13], CoSe [14], CoFe [15], and other related compounds, have garnered significant attention as a promising research area for low-cost and high-efficiency OER catalysts. Cobalt-based materials have unique electronic structures and abundant active sites. Currently, the methods to improve the OER performance of cobalt-based materials mainly include increasing the active sites by doping and adjusting the surface electronic structure or synergy by constructing heterostructures, thereby improving the electrocatalytic activity of the materials. Ke Zhang et al. doped $CoSe_2$ with iron by hydrothermal synthesis, and the resulting the $FeCoSe_2$ /$Co_{0.85}$ Se heterostructure catalyst exhibited good electrocatalytic activity at a current density of 10 $mA \cdot cm^{-2}$. The overpotential under-density is 0.33 V, and the Tafel slope is 50.8 $mV \cdot dev^{-1}$ [16]. Yucan Dong et al. obtained the excellent OER performance of Co_9S_8@CoS_2 heterojunctions synthesized by hydrogen etching of CoS_2, and the Co_9S_8@CoS_2 heterostructures were dynamically reformed during OER with the in situ formation of CoOOH structure, thus exhibiting excellent electrocatalytic performance [17]. It can be seen that constructing heterostructures on cobalt-based materials is a common method to improve carrier mobility and thus improve electrocatalytic performance [18,19].

In recent years, we have witnessed the eutrophication of many water bodies due to pollution and biological invasions of the ecological environment. These factors cause algal blooms in some areas and severe ecological and environmental problems. On the other hand, the development and utilization of algae can turn waste into treasure and provide new ideas for developing and utilizing new energy. In this paper, kelp was used as the carbon precursor, and it was doped with nitrogen to design and synthesize the cobalt selenide composite heterojunction. The material's electrochemical test showed that the OER process' overpotential was 292 mV; the Tafel slope was 98.71 $mV \cdot dev^{-1}$; and the electrochemical impedance was 125.95 Ω. The mechanism of the enhancement of the electrocatalytic activity by the heterostructure was further studied through theoretical calculations. These calculations confirm that the presence of the biomass carbon substrate enhances the charge transport of the OER process and promotes the OER process [20].

2. Experimental Section

2.1. Catalyst Preparation

The kelp was purchased from a local supermarket in Changzhou, China. Melamine ($C_3H_6N_6$), potassium hydroxide (KOH) and cobalt acetate tetrahydrate provided by Sinopharm Chemical Reagent Co., Ltd. (Shanghai, China), selenium powder (China Institute of Metal Materials), tube furnace (Anhui Jing Branch Co., Ltd. Hefei, China), and electrochemical workstation (CS350H, Wuhan Coster Co., Ltd. Wuhan, China) were used. Deionized water was used in all of the experiments.

Synthesis of NC: NC was synthesized following a combustion technique. First, 5 g of kelp was cut into pieces, washed, and mixed with KOH in a beaker. Ethanol was added to the beaker, and the mixture was then subjected to ultrasonic drying for 1 h, followed by vacuum-drying at 80 °C for 1 h. The mixture was transferred to a crucible and heated to 550 °C in a tube furnace at a heating rate of 5 °C·min^{-1}, kept warm for 2 h, and then washed to neutrality after cooling. A reddish powder was obtained. A certain amount

of melamine was added to the reddish powder in a beaker, followed by the addition of ethanol to dissolve it. The mixture was ultrasonicated for 1 h and vacuum-dried at 80 °C. The mixture was heated to 900 °C in a tube furnace at a heating rate of 5 °C·min^{-1}, kept warm for 2 h, cooled, and dried to obtain a black powder. As a comparison, the amounts of melamine added were 6 g, 12 g, and 16 g, respectively, and the samples were marked as NC@X (X = 1, 2, 3). The schematic flow chart of this experiment is shown in Figure 1.

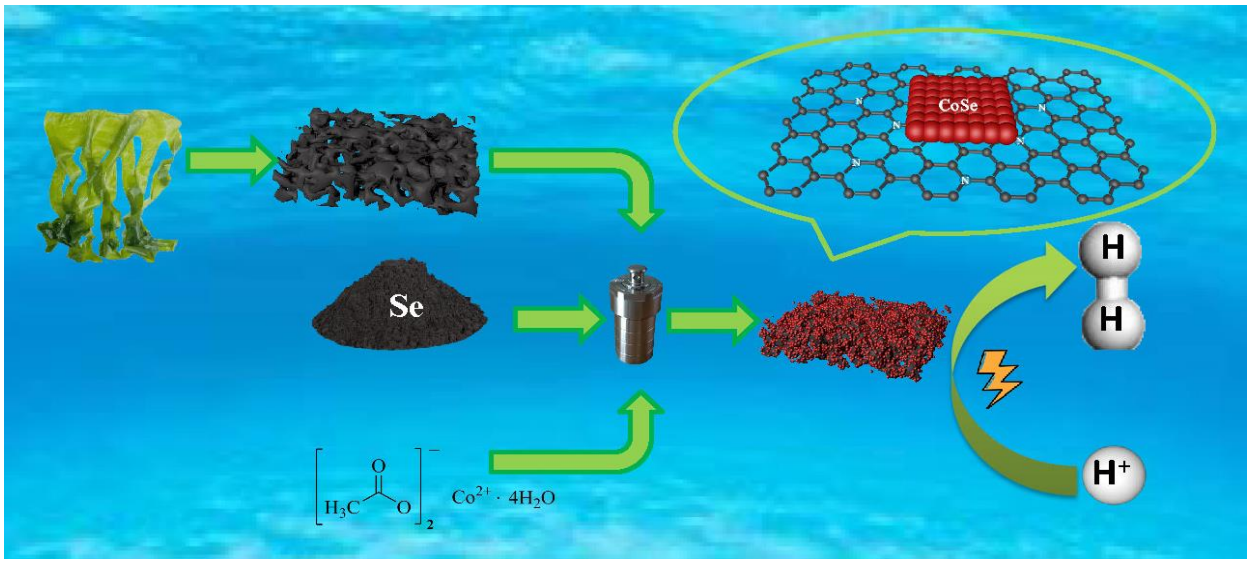

Figure 1. Schematic illustration of the synthesis of CS/yNC@X.

Preparation of CS/yNC@X: A nitrogen-doped biomass carbon-based composite cobalt selenide heterojunction was synthesized using a solvothermal method. An appropriate amount of NC@X, selenium powder, cobalt acetate tetrahydrate, sodium borohydride, and 23 mL of absolute ethanol was placed in a 50 mL hydrothermal kettle and kept at 180 °C for 18 h. After cooling, the sample was rinsed with deionized water and absolute ethanol, dried, and finally obtained as a black powder. For comparison, samples with 0.05 g, 0.1 g, and 0.2 g of NC@X added were labeled as CS/yNC@X (y = 1, 2, 3).

Preparation of CoSe: Cobalt selenide was combined using the solvothermal method. First, we took an appropriate amount of selenium powder, cobalt acetate tetrahydrate, sodium borohydride, and 23 mL of absolute ethanol. We put them in a 50 mL hydrothermal kettle to keep warm at 180 °C for 18 h, then washed them with deionized water and absolute ethanol after cooling down. Finally, they were dried to obtain a black powder.

2.2. Theoretical Calculations

All calculations were performed using the Dmol3 module from Materials Studio 2020. The GGA/PBE functional was used in the DFT simulation, and the double value plus polarization basis set was used. The isoelectronic calculation of the complex showed that the spin state of the system had no spin limitation, and the SCF self-consistent convergence accuracy was 1.0×10^{-6}. The allowable deviations for the total energy, gradient, and displacement were 1.0×10^{5} Ha, 0.002 Ha·Å^{-1}, and 0.005 Å, respectively. In order to avoid the influence of Brillouin zone sampling, the k point was set to $3 \times 3 \times 1$ to ensure the rationality of the calculation results.

2.3. Physical Characterization

The crystal phase of the catalyst was characterized by X-ray. Its morphology was characterized by scanning electron (Nova450) and transmission electron (TEM) (Jem2100 F), and its chemical composition and elemental valence states were determined by X-ray photoelectron spectroscopy (Brooke D8 advance).

2.4. Electrochemical Measurements

The electrochemical performance of the prepared product was tested using the method of manufacturing powder electrodes. First, the reference electrode was converted to a standard hydrogen electrode (SHE) using the conversion formula:

$$E\{RHE\} = E\{SCE\} + 0.243\ V + 0.0591 \times pH \quad (1)$$

Next, a uniformly dispersed coating solution was obtained by dispersing 2 mg of catalyst in 360 μL isopropanol, 120 μL water, and 20 μL Nafion (5 wt%) and then sonicating the mixture for 20 min. Then, 12 μL of the obtained solution was coated on a 3 mm glassy carbon electrode and dried, forming the desired powder electrode. The electrochemical test was carried out using an electrochemical workstation (CS350H, Wuhan Kesite Instrument Co., Ltd., Wuhan, China) and a 1 M KOH solution (pH = 14). The volt–ampere characteristic curve was scanned at a speed of 5 $mV \cdot s^{-1}$ and the electrochemical impedance spectroscopy test was carried out under 5 mV AC voltage, with the scanning frequency ranging from 0.1 Hz to 105 Hz. To determine the stability of the catalyst, the voltage of −0.5 V was scanned for 14 h to record the current change.

3. Results

The microstructures of CS/1NC@X were investigated using SEM. Figure 2 showed that CS/1NC@X had a distinct three-dimensional coral-like structure. The three-dimensional coral-like structure of CS/1NC@X in the figure is composed of cobalt selenide particles tens of nanometers in size. Cobalt selenide is complexed with NC@X through various forms such as intercalation, loading, and encapsulation, among which the loading type is dominant. In the overall structure, NC@X acts as a carrier for CoSe loading and fixes CoSe into a closely packed structure.

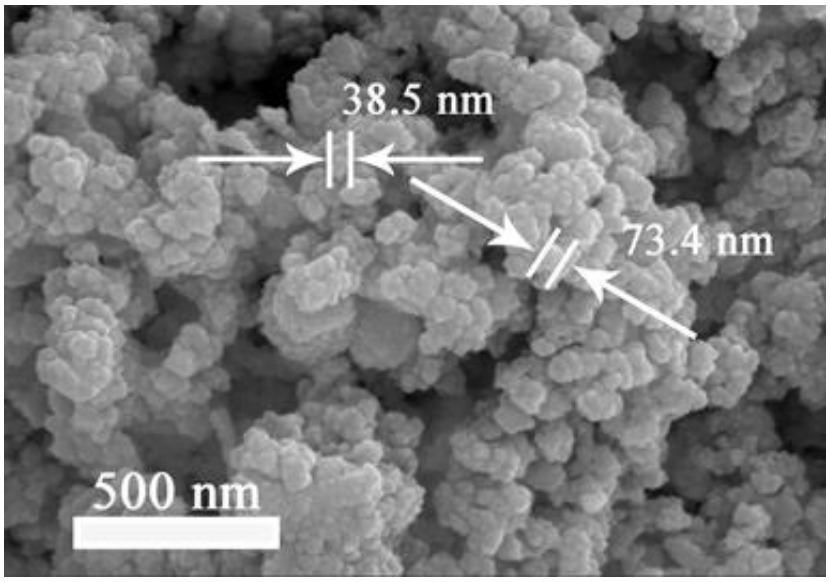

Figure 2. SEM images of CS/1NC@3.

From the TEM and HRTEM results of CS/1NC@3 (Figure 3a,b), it can be clearly observed that the nano-substrate structure of NC is uniformly loaded with CoSe nanoparticles to form a heterostructure. This helps to facilitate quick electron transfer from NC@X to CoSe, thereby improving the material's conductivity and surface binding energy and accelerating the electrocatalytic process. In high-resolution TEM (HRTEM) images, lattice spacings of 0.323 nm, 0.271 nm, and 0.218 nm were determined, corresponding to the CoSe (1 0 0), (1 0 1), and (1 0 2) crystal planes, respectively. The interlayer spacing is close to the

ideal spacing, indicating that the degree of graphitization of the NC substrate after firing is higher, and the conductivity is enhanced [21].

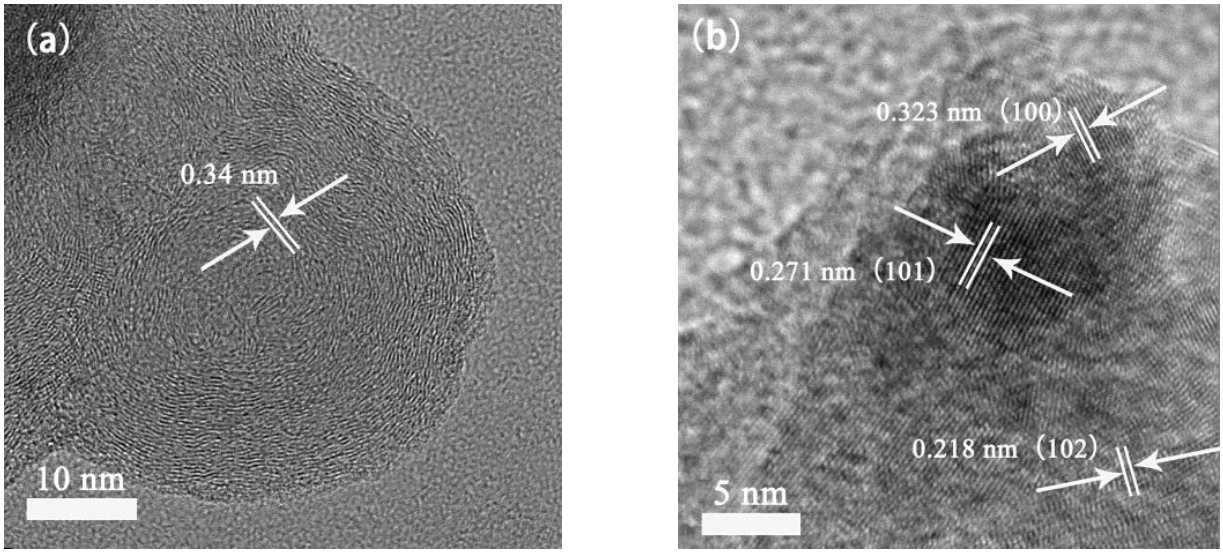

Figure 3. TEM image (**a**) and HRTEM image (**b**) of CS/1NC@3.

The results of X-ray powder diffraction (Figure 4) show that there are three strong diffraction peaks in Figure 4, which correspond to the (1 0 0) plane, (1 0 1) plane, and (1 0 2) plane of CoSe, respectively. Specifically, the (1 0 1) plane shows a strong diffraction peak intensity, which is attributed to the fact that it is the active plane of CoSe. In addition, the NC@X diffraction peak appears on CoSe, and the (1 0 0) peak corresponding to the carbon material shifts to the left. This indicates that after N doping, the increase in the interlayer spacing leads to the change in the energy band filling state and the Fermi energy level, which enhances the conductivity, ion transport ability, and catalytic activity of the material. The increase in the interlayer spacing can expose more active sites and unsaturated defect sites, which can effectively improve the electrocatalytic performance [22–24]. Calculated by Scherrer's formula, the average grain size of CoSe was 19.3 nm and the average grain size of CS/1NC@3 was 28.3 nm. This shows that CoSe and NC@3 form a heterostructure and promote the formation of CS/1NC@3 phase.

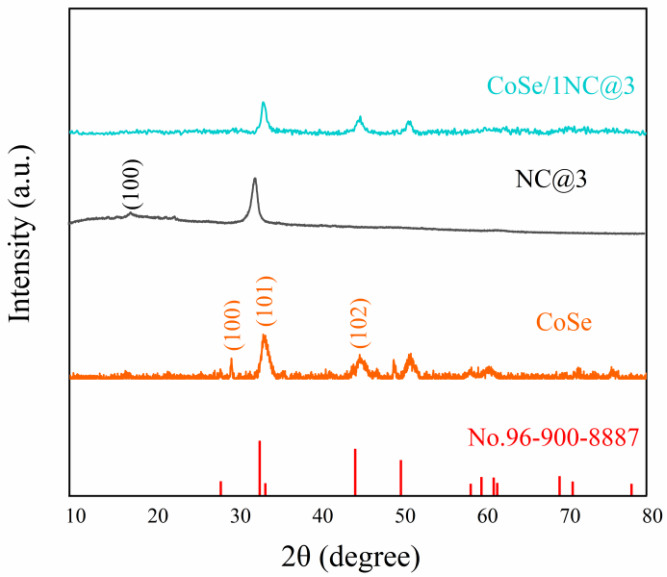

Figure 4. XRD pattern of CS/1NC@3, CoSe, NC@3.

The chemical states and bonding structures of CS/1NC@3 and their components were investigated by X-ray Photoelectron Spectroscopy (XPS) (Figure 5a–d). The high-resolution C 1s spectrum of CoSe/NC can be decomposed into peaks: C-C (284.8 eV), N-C (290.8 eV) and C-O (286.4 eV). Nitrogen is doped into the skeleton of kelp carbon by co-calcination, with a N-to-C ratio of approximately 1:6. Since nitrogen atoms are more electronegative than carbon atoms, nitrogen-doped carbon materials will have better electronic conductivity. After nitrogen atoms are doped into the carbon material framework, they can provide more free electrons for the conduction band, significantly improving the electrical conductivity of the carbon framework [25]. N 1s can be decomposed into two peaks at 397.8 eV and 405.7 eV, respectively, for the pyridinic nitrogen and N-O structures. These are related to the small amount of oxygen contained in kelp itself, which may be partially oxidized during the calcination process. In addition, Co 2p is affected by orbital hybridization and can be decomposed into Co 2p3/2 and Co 2p1/2. The valence state of the element is mainly +2. Compared with pure CoSe, the binding energy shifts to the low energy direction by about 0.25 eV, and the binding energy of the C-C bond can also shift to the high-energy direction by about 0.2 eV, which shows that in the CoSe/NC heterojunction, there is a strong electronic coupling between the CN structure of the substrate and CoSe. The charge transport direction is CN-Co. The CN structure of the substrate injects a small number of electrons into CoSe, thus improving its activity [26,27]. Se is decomposed into two electron orbitals, Se 3d5/2 (54.4 eV) and Se 3d3/2 (60.1 eV), which exist in the form of CoSe conjugates.

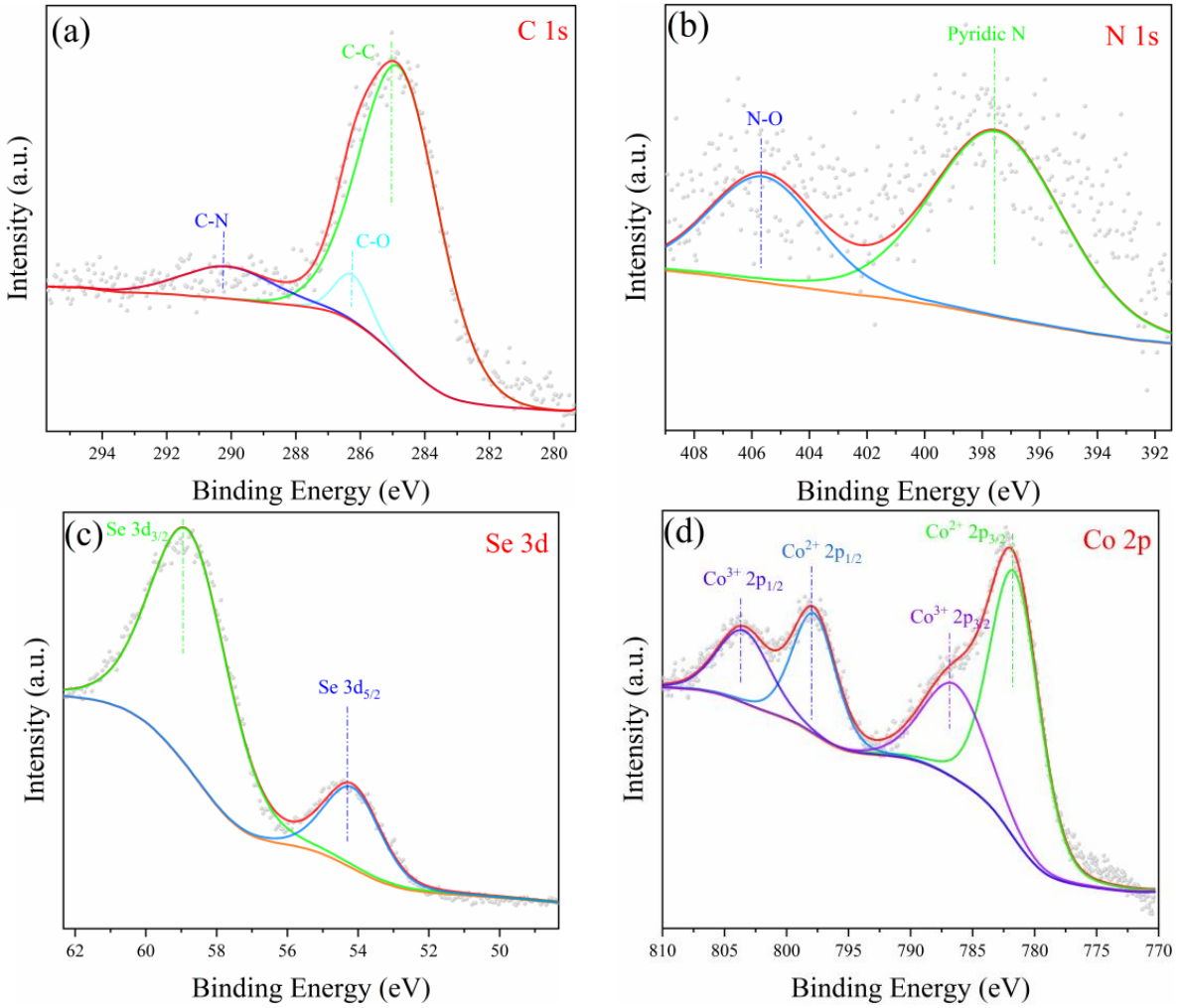

Figure 5. XPS spectra of C 1s (**a**), N 1s (**b**), Se 3d (**c**), and Co 2p (**d**) spectra for CS/1NC@3.

The presence of multiple oxygen-containing functional groups on the surface of carbon materials can promote the strong adsorption of metal particles, resulting in an improved dispersion of the metal particles [4]. The CS/1NC@3 was further investigated by Fourier transform infrared (FTIR) spectroscopy. The FTIR spectrum of CS/1NC@3 exhibited peaks at 3380 cm^{-1}, 2925 cm^{-1}, 1627 cm^{-1}, 1385 cm^{-1}, and 1045 cm^{-1}, which were attributed to the -OH, C-H, C=N, C=O and C=N functional groups, respectively (Figure 6). The infrared spectrum showed that the oxygen-containing functional groups on the material may be phenolic hydroxyl, carboxyl, lactone, or carbonyl [28]. However, the presence of a small amount of oxygen-containing groups can increase surface wetting reactivity and electrochemical performance.

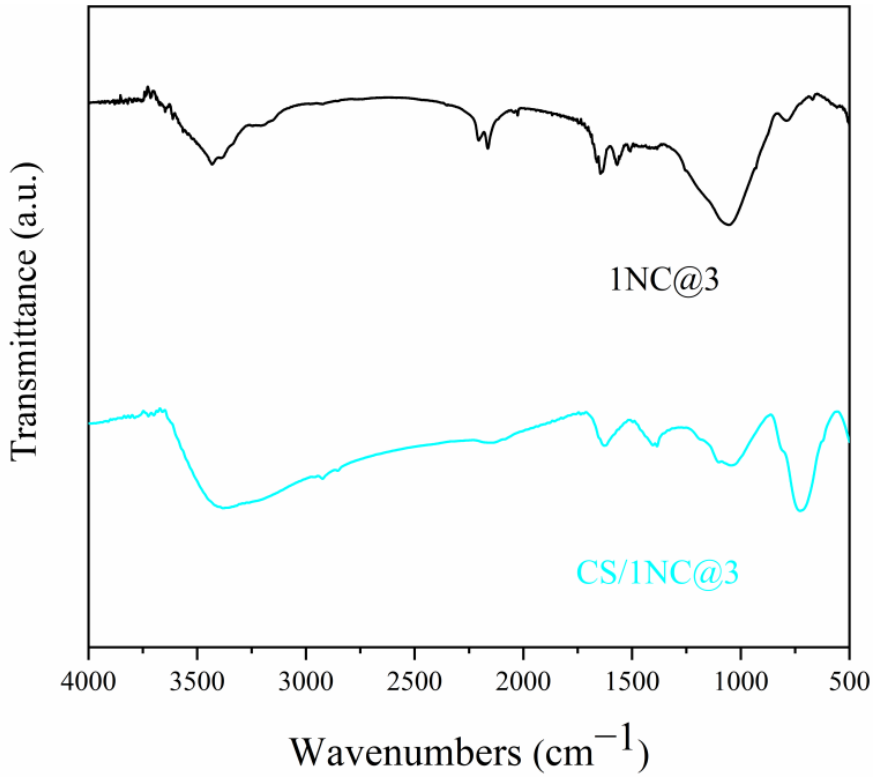

Figure 6. FTIR spectra of the CS/1NC@3 and NC@3.

The electrochemical performance test results of CS/1NC@3 materials are shown in Figure 7a–c. As can be seen from the linear sweep voltammetry (LSV) curve, the overpotential of CS/1NC@3 is the lowest, which is 292.7 mV at a current density of 10 $mA \cdot cm^{-2}$, while that of pure CoSe is 384.8 mV. This demonstrates that CoSe and N-doped biochar have formed a heterostructure, which increases the charge carrier mobility and exhibits superior electrocatalytic activity compared to the original CoSe [29]. At the same time, the influence of the NC substrate-modified CoSe electrode on the kinetics of the electrocatalytic OER reaction was analyzed by the Tafel diagram, in which the Tafel slope (98.71 $mV \cdot dec^{-1}$) of CS/1 NC@3 was smaller than that of CoSe (258.31 $mV \cdot dec^{-1}$). The decrease in the Tafel slope indicates that the addition of NC changes the rate-determining step but plays a certain role in enhancing the kinetic process of the electrochemical OER. To further explore the reason for the enhanced activity, the EIS of the material was tested from the perspective of charge transfer kinetics. The results of electrochemical impedance analysis showed that, compared with CoSe (300.54 Ω), CS/1NC@3 (125.95 Ω) composites had smaller charge transfer resistance and thus higher activity [30].

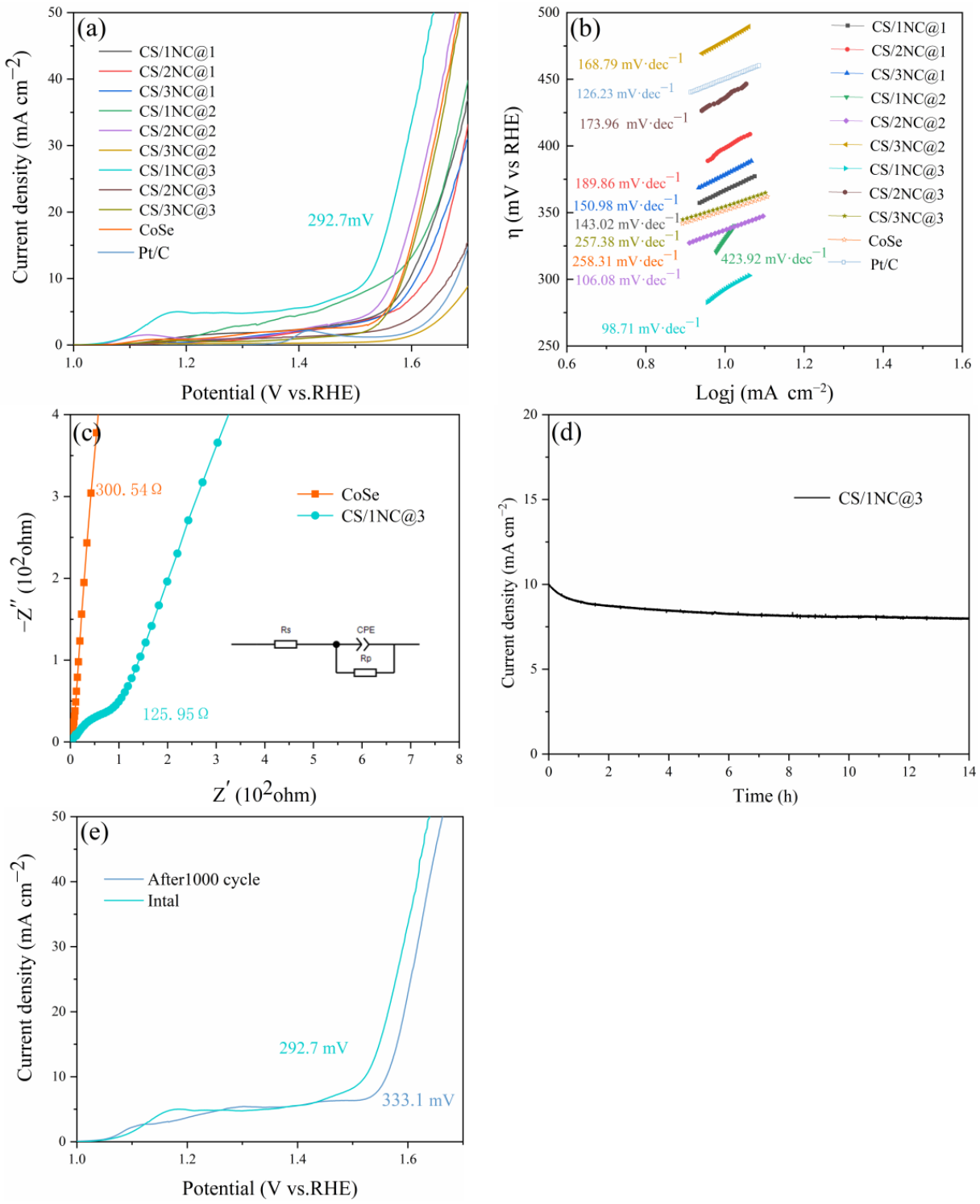

Figure 7. (**a**) LSV curve (without iR-corrected) and (**b**) Tafel slope of CS/yNC@X, (**c**) Nyquist plots of CS/1NC@3 and CoSe, (**d**) i–t curves of CS/1NC@3. (**e**) LSV curves of CS/1NC@3 in 1 M KOH solutions, respectively, before and after 1000 cycles.

The CS/1NC@3 catalyst was kept in 1 M KOH for 14 h in Figure 7d, which indicated that the heterojunction formed between cobalt selenide and biochar material by the hydrothermal method had good stability under alkaline conditions. In Figure 7e, we examined the stability of the catalytic electrode CS/1NC@3 LSV curves after 1000 consecutive CV cycle values remained at 333.1 mV, which further confirmed the high stability

of CS/1NC@3. This high stability can be attributed to the strong bond between NC@3 and CoSe.

DFT calculation: Generally, a good electrocatalyst has excellent charge capture and transfer capabilities; the key lies in the electronic structure and conductivity of the catalyst. Based on the XPS surface element analysis results, a heterostructure model was constructed using Materials Studio. The (0 0 1) surface of CoSe was chosen as the active surface, and a 2 × 2 supercell was created in the X and Y directions. The lattice lengths of CoSe after the supercell expansion in the X and Y directions were 7.21 Å, while that of CN was 7.38 Å. The overall lattice mismatch degree after constructing the heterojunction was less than 5%, which is considered reasonable. Based on the density of states (DOS) diagrams of CS/yNC@X and the CoSe catalyst depicted in Figure 8a, b, respectively, the d-band theory suggests that when the d-band center of the transition metal is positioned closer to the Fermi level, the anti-bonding orbital located above the Fermi level becomes elevated after the catalyst and the adsorbate orbital form a bond. As a result, there is a reduced probability of electron filling in the anti-bonding orbital, which leads to more stable adsorption, stronger adsorption energy, and enhanced catalytic activity [31]. From the PDOS plot of CS/yNC@X, it can be observed that the heterostructure still exhibits strong metallic properties after doping with nitrogen. The enhanced metallic properties of the biomass-based carbon matrix after nitrogen doping indicate that this doping method can improve the system's conductivity, which is beneficial for promoting electrochemical reactions. The d-band center of pure CoSe is at 2.14 eV, and the CS/1NC@3 d-band center is at2.093 eV after projecting the polarized density of the state of CS/1NC@3 to the Fermi surface. The center is obviously shifted to the Fermi level. It is clear that the activity of the CoSe material is significantly enhanced by the method of constructing a heterojunction, and the OER reaction is better promoted, which is consistent with the experimental results.

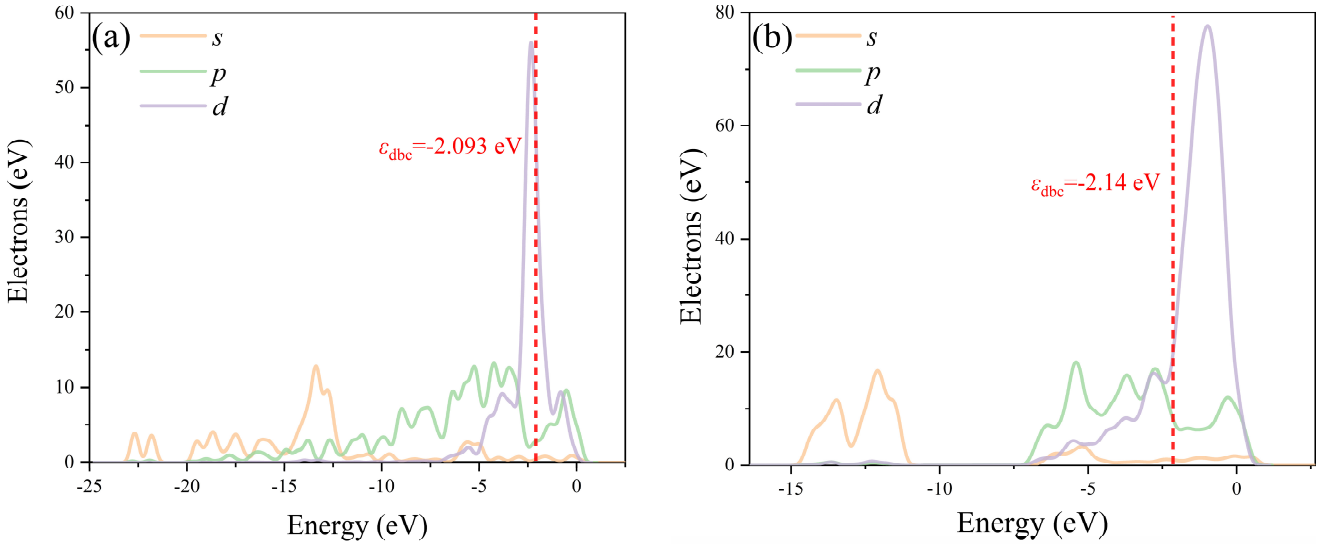

Figure 8. (**a**) CS/yNC@X density of states diagram, (**b**) CoSe density of states diagram.

Through the calculation of the differential charge of the material, a section perpendicular to the heterojunction material is constructed along the A B direction, and the heterostructure model constructed by Materials Studio and the section diagram of the average differential charge density of the material along the Z direction are obtained. Figure 9b, c. It is clear that the direction of charge transfer is from the carbon-nitrogen substrate to CoSe, and the charge is concentrated at the Co atom (the red part in the figure). Co has a higher catalytic activity after receiving electrons, which is consistent with the current general conclusions. Gaining electrons promotes the reactivity of metals [32–34]. The electrostatic potential analysis also shows that the doping of nitrogen improves the

conductivity of the carbon-based substrate and that there is a charge transfer from C to N inside the carbon–nitrogen substrate.

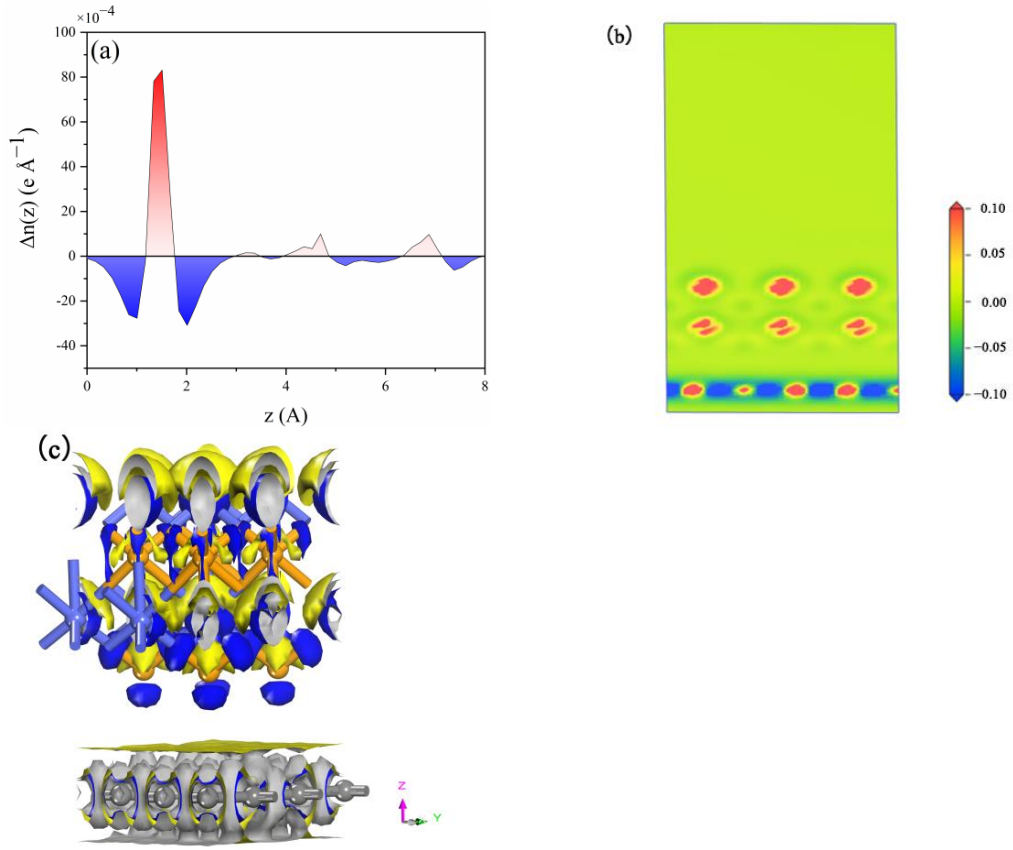

Figure 9. (**a**) CS/yNC@X differential charge density map, (**b**) CS/yNC@X differential charge section map, (**c**) heterostructure electrostatic potential distribution map.

The four-electron process is Nørskov's classical theory, and this process is currently generally accepted in academia [35,36]. According to the four-electron process of OER [37,38], the decomposition of water on the catalyst proceeds in four steps:

$$\text{Catalyst} + H_2O = {}^*OH + H^+ + e^- \quad (2)$$

$${}^*OH = {}^*O + H^+ + e^- \quad (3)$$

$${}^*O + H_2O = {}^*OOH + H^+ + e^- \quad (4)$$

$${}^*OOH = * + O_2 + H^+ + e^- \quad (5)$$

In order to calculate the energy of each step correctly, the initial adsorption configuration was optimized, as shown in Figure 10a–d. There were three possible adsorption active centers on CoSe: Co inside, Se, and Co on edge. These three sites were used as active centers to calculate the energy and configuration changes of the adsorbed OH. After the adsorption of OH by marginal Co, the overall energy is the lowest, which is −219.18 eV), making it the most likely site at which OER will occur. After the adsorption of OH by internal Co, the overall energy is −219.03 eV. In comparison, the overall energy after the adsorption of OH by Se as the active center is −218.12 eV, which is the highest amount of energy. It is difficult for OH adsorption to occur at the Se site. By analyzing the bond length between the three types of active centers and O after the adsorption of OH, it can be

found that the adsorption energy of OH adsorbed by the edge Co is more negative, so the distance between Co-O is closer, which is 1.8 Å. After the adsorption of OH by the internal Co, the Co-O distance is 2.08 Å. After the adsorption of OH by Se, the OH tends to be far away from Se and close to Co after structural optimization. It is difficult for surface OH to adsorb on the Se surface, and the Se-O distance of 3.14 Å also indicates that Se is not the active center of the OER process. The adsorption energy of marginal Co is greater than that of internal Co, which may be due to the exposure of more coordination sites of marginal Co. Therefore, the calculation of the four-electron process step diagram uses marginal Co as the active site to expand the calculation.

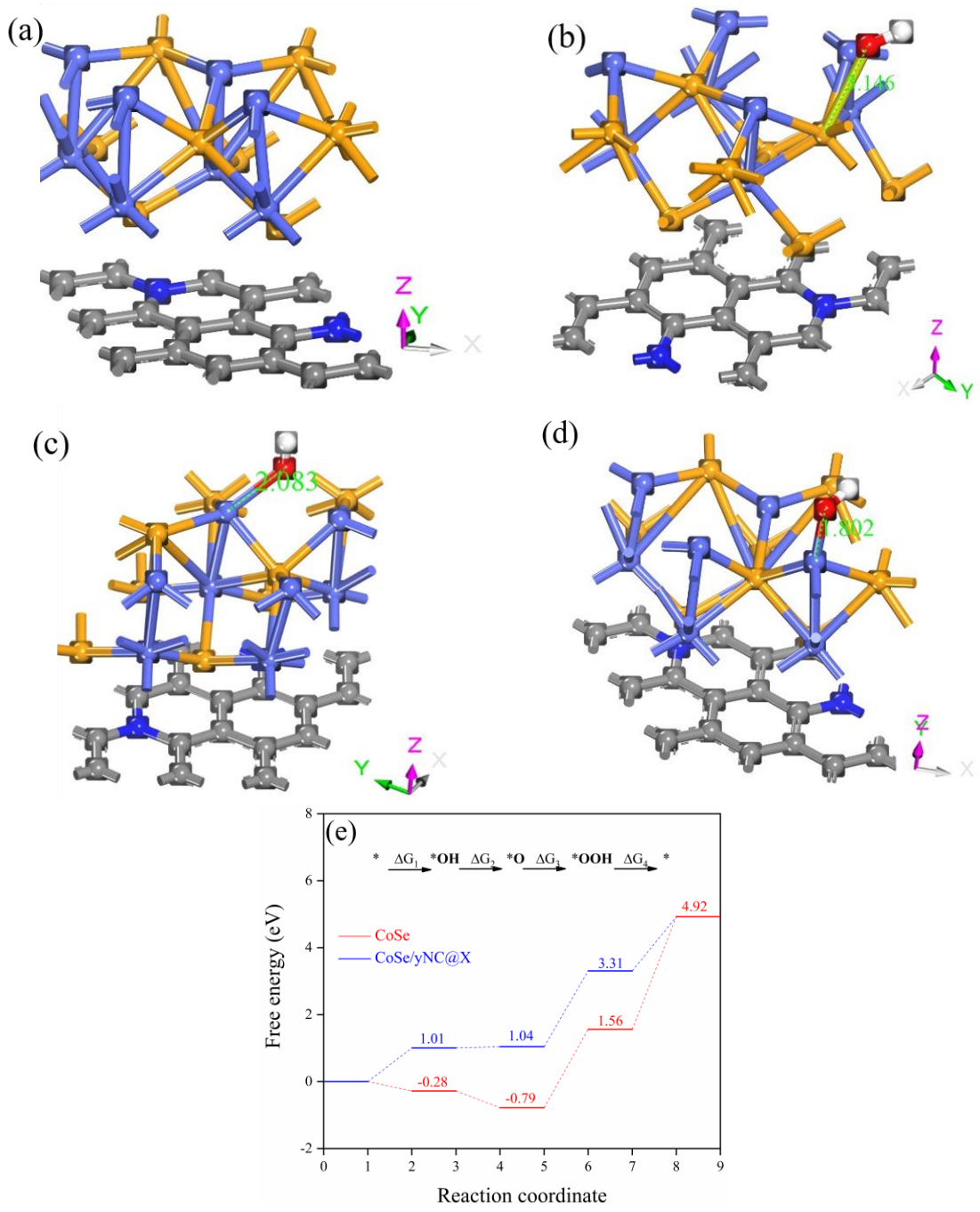

Figure 10. (**a**–**d**) are four simulated configurations, (**e**) OER process step diagram of CoSe and CoSe/yNC@X.

The free energy of each reaction step of pure CoSe and CS/yNC@X catalyst OER was calculated, as shown in Figure 10e. The change of free energy evaluated the intrinsic activity of the catalyst, and the change of free energy of pure CoSe and the CS/yNC@X catalyst OER process were compared. The free energy of the second and third steps of pure CoSe changes greatly, which seriously affects the reaction rate. *OH is converted to *O in the second step of the final speed step, and the energy barrier is as high as 3.25 eV, which makes it difficult to carry out the kinetic process of water electrolysis catalyzed by pure CoSe. The rate-determining step of the CS/yNC@X heterojunction is the formation of the second step, OOH intermediate, with an energy barrier of 1.42 eV. Therefore, by synthesizing heterojunction materials, the kinetic process of the catalyst surface reaction is changed, the velocity step is changed, and the energy barrier of the rate-determining step is effectively reduced, thus improving the performance of OER.

4. Conclusions

Utilizing Marine biomass, through the two-step carbonization and solvothermal synthesis methods, with selenium powder as the selenium source, cobalt acetate tetrahydrate as the cobalt source, kelp as the carbon precursor, KOH activation, and using melamine as the nitrogen source, carbon/heterojunction composites containing rich nitrogen doping were prepared. The strong interfacial interaction of the two components can establish abundant high-speed electron transmission channels. The synthesized material has CS/1NC@3 biomass porous carbon structure and abundant active sites. Through XPS analysis and other characterization methods, the element composition of the surface and the electron transfer method were judged, and the synthesized material was finally confirmed as CS/1NC@3. According to the electrochemical performance test and characterization, under the current density of 10 $mA{\cdot}cm^{-2}$, the required overpotential is 292.7 mV, and the Tafel slope is 98.71 $mV{\cdot}dev^{-1}$. Compared with CoSe alone, the center of the D-band shifts towards the Fermi surface, demonstrating enhanced catalytic activity. According to the results of the step diagram of the four-electron process, by directly doping nitrogen with carbon substrate, the overpotential of the process was significantly reduced, and the OER process was promoted. CS/1NC@3 showed significantly enhanced OER activity, which was consistent with the theoretical settlement results.

Author Contributions: L.W. (Longyao Wang), L.W. (Lan Wang); Y.Z. (Yupei Zhao) and P.W. planned and supervised this work; T.M. and F.A. prepared the multilayer films and co-wrote and edited this paper with Y.Z. (Yupei Zhao); Y.Z. (Yupei Zhao) and P.W. supervised the Masters student T.M. and F.A. performed some experiments and tests; T.M. and H.S. performed and analyzed characterization of materials and samples; Y.Z. (Yujun Zhu) and Y.L. provided simulations and calculations. All authors have read and agreed to the published version of the manuscript.

Funding: National Natural Science Foundation of China, No. 22072007. The Jiangsu Province Project of Industry-University-Research Cooperation, No. BY20221141. Jiangsu Graduate Research and Practice Innovation Program, No. SJCX21_1252. Jiangsu College Student Innovation and Entrepreneurship Training Program, No. 202210292097Y. Zhenjiang Key Research and Development Program (Industry Foresight and Common Key Technologies), No. CQ2022006. Jiangsu Engineering Technology Research Center for Novel Anti-Influenza Virus Drugs, Jiangsu Graduate Workstation, Zhenjiang Salicylic Acid Series Products Engineering Technology Research Center, Zhenjiang Municipal Enterprise Technology Center.

Institutional Review Board Statement: Not applicable.

Informed Consent Statement: Not applicable.

Data Availability Statement: Not applicable.

Acknowledgments: The author is immensely grateful to Shuo Li for his assistance with English writing and Chengdong Wang for his help in the experiment.

Conflicts of Interest: The authors declare no conflict of interest.

References

1. Gao, Y.; Zhang, N.; Wang, C.; Zhao, F.; Yu, Y. Construction of Fe_2O_3@CuO Heterojunction Nanotubes for Ellen Vayner hanced Oxygen Evolution Reaction. *ACS Appl. Energy Mater.* **2019**, *3*, 666–674. [CrossRef]
2. Basu, M.; Zhang, Z.W.; Chen, C.J.; Lu, T.H.; Hu, S.F.; Liu, R.S. $CoSe_2$ Embedded in C_3N_4: An Efficient Photocathode for Photoelectrochemical Water Splitting. *ACS Appl. Mater. Inter.* **2016**, *8*, 26690–26696. [CrossRef] [PubMed]
3. Campos-Roldán, C.A.; Alonso-Vante, N. The Oxygen Reduction and Hydrogen Evolution Reactions on Carbon Supported Cobalt Diselenide Nanostructures. *J. Electrochem. Soc.* **2020**, *167*, 026507. [CrossRef]
4. Ye, Y.-Y.; Qian, T.-T.; Jiang, H. Co-Loaded N-Doped Biochar as a High-Performance Oxygen Reduction Reaction Electrocatalyst by Combined Pyrolysis of Biomass. Ind. Engineering. *Chem. Res.* **2020**, *59*, 15614–15623.
5. Ma, L.L.; Hu, X.; Liu, W.J.; Li, H.C.; Lam, P.K.S.; Zeng, R.J.; Yu, H.Q. Constructing N, P-dually doped biochar materials from biomass wastes for high-performance bifunctional oxygen electrocatalysts. *Chemosphere.* **2021**, *278*, 130508. [CrossRef]
6. Ma, N.; Jia, Y.; Yang, X.; She, X.; Zhang, L.; Peng, Z.; Yao, X.; Yang, D. Seaweed biomass derived (Ni,Co)/CNT nanoaerogels: Efficient bifunctional electrocatalysts for oxygen evolution and reduction reactions. *J. Mater. Chem. A* **2016**, *4*, 6376–6384. [CrossRef]
7. Sekar, S.; Sim, D.H.; Lee, S. Excellent Electrocatalytic Hydrogen Evolution Reaction Performances of Partially Graphitized Activated-Carbon Nanobundles Derived from Biomass Human Hair Wastes. *Nanomaterials.* **2022**, *12*, 531. [CrossRef]
8. Huang, N.-B.; Zhang, J.-J.; Sun, Y.; Sun, X.-N.; Qiu, Z.-Y.; Ge, X.-W. A non-traditional biomass-derived N, P, and S ternary self-doped 3D multichannel carbon ORR electrocatalyst. *New J. Chem.* **2020**, *44*, 14604–14614. [CrossRef]
9. Pérez-Salcedo, K.Y.; Alonso-Lemus, I.L.; Quintana, P.; Mena-Durán, C.J.; Barbosa, R.; Escobar, B. Self-doped Sargassum spp. derived biocarbon as electrocatalysts for ORR in alkaline media. *Int. J. Hydrogen Energy.* **2019**, *44*, 12399–12408. [CrossRef]
10. Wang, F.; Li, Q.; Xiao, Z.; Jiang, B.; Ren, J.; Jin, Z.; Tang, X.; Chen, Y.; Li, X. Conversion of rice husk biomass into electrocatalyst for oxygen reduction reaction in Zn-air battery: Effect of self-doped Si on performance. *J. Colloid Interface Sci.* **2022**, *606*, 1014–1023. [CrossRef]
11. Hao, Y.; Zhang, X.; Yang, Q.; Chen, K.; Guo, J.; Zhou, D.; Feng, L.; Slanina, Z. Highly porous defective carbons derived from seaweed biomass as efficient electrocatalysts for oxygen reduction in both alkaline and acidic media. *Carbon* **2018**, *137*, 93–103. [CrossRef]
12. Xu, J.; Li, J.; Lian, Z.; Araujo, A.; Li, Y.; Wei, B.; Yu, Z.; Bondarchuk, O.; Amorim, I.; Tileli, V.; et al. Atomic-Step Enriched Ruthenium–Iridium Nanocrystals Anchored Homogeneously on MOF-Derived Support for Efficient and Stable Oxygen Evolution in Acidic and Neutral Media. *ACS Catal.* **2021**, *11*, 3402–3413. [CrossRef]
13. Zhan, Y.; Yu, S.Z.; Luo, S.H.; Feng, J.; Wang, Q. Nitrogen-Coordinated CoS_2@NC Yolk-Shell Polyhedrons Catalysts Derived from a Metal-Organic Framework for a Highly Reversible Li-O_2 Battery. *ACS Appl. Mater. Inter.* **2021**, *13*, 17658–17667. [CrossRef] [PubMed]
14. Sobhani, A.; Salavati-Niasari, M. Cobalt selenide nanostructures: Hydrothermal synthesis, considering the magnetic property and effect of the different synthesis conditions. *J. Mol. Liq.* **2016**, *219*, 1089–1094. [CrossRef]
15. Dang, N.K.; Tiwari, J.N.; Sultan, S.; Meena, A.; Kim, K.S. Multi-site catalyst derived from Cr atoms-substituted CoFe nanoparticles for high-performance oxygen evolution activity. *Chem. Eng. J.* **2021**, *404*, 12653. [CrossRef]
16. Zhang, K.; Shi, M.; Wu, Y.; Wang, C. Constructing $FeCoSe_2$/$Co_{0.85}Se$ heterostructure catalysts for efficient oxygen evolution. *J. Alloys Compd.* **2020**, *825*, 154073. [CrossRef]
17. Dong, Y.; Ran, J.; Liu, Q.; Zhang, G.; Jiang, X.; Gao, D. Hydrogen-etched CoS_2 to produce a Co_9S_8@CoS_2 heterostructure electrocatalyst for highly efficient oxygen evolution reaction. *RSC Adv.* **2021**, *11*, 30448–30454. [CrossRef] [PubMed]
18. Tang, Y.; Jing, F.; Xu, Z.; Zhang, F.; Mai, Y.; Wu, D. Highly Crumpled Hybrids of Nitrogen/Sulfur Dual-Doped Graphene and Co9S8 Nanoplates as Efficient Bifunctional Oxygen Electrocatalysts. *ACS Appl. Mater. Interfaces.* **2017**, *9*, 12340–12347. [CrossRef]
19. Feizi, H.; Bagheri, R.; Song, Z.; Shen, J.-R.; Allakhverdiev, S.I.; Najafpour, M.M. Cobalt/Cobalt Oxide Surface for Water Oxidation. *ACS Sustain. Chem. Eng.* **2019**, *7*, 6093–6105. [CrossRef]
20. Wu, Y.; Wang, F.; Ke, N.; Dong, B.; Huang, A.; Tan, C.; Yin, L.; Xu, X.; Hao, L.; Xian, Y.; et al. Self-supported cobalt/cobalt selenide heterojunction for highly efficient overall water splitting. *J. Alloys Compd.* **2022**, *925*, 166683. [CrossRef]
21. Lian, P.; Zhu, X.; Liang, S.; Li, Z.; Yang, W.; Wang, H. Large reversible capacity of high quality graphene sheets as an anode material for lithium-ion batteries. *Electrochim. Acta.* **2010**, *55*, 3909–3914. [CrossRef]
22. Liang, H.; Jia, L.; Chen, F.; Jing, S.; Tsiakaras, P. A novel efficient electrocatalyst for oxygen reduction and oxygen evolution reaction in Li-O_2 batteries: Co/CoSe embedded N, Se co-doped carbon. *Appl. Catal. B* **2022**, *317*, 121698. [CrossRef]
23. Zhang, T.; Yu, J.; Guo, H.; Liu, J.; Liu, Q.; Song, D.; Chen, R.; Li, R.; Liu, P.; Wang, J. Heterogeneous $CoSe_2$–CoO nanoparticles immobilized into N-doped carbon fibers for efficient overall water splitting. *Electrochim. Acta* **2020**, *356*, 136822. [CrossRef]
24. Xue, Y.; Zhang, Q.; Wang, W.; Cao, H.; Yang, Q.; Fu, L. Opening Two-Dimensional Materials for Energy Conversion and Storage: A Concept. *Adv. Energy Mater.* **2017**, *7*, 1602684. [CrossRef]
25. Sheng, Z.; Shao, L.; Chen, J.; Bao, W.; Wang, F.; Xia, X. Catalyst-Free Synthesis of Nitrogen-Doped Graphene via Thermal Annealing Graphite Oxide with Melamine and Its Excellent Electrocatalysis. *ACS Nano.* **2011**, *5*, 4350–4358. [CrossRef]
26. Sam, D.K.; Sam, E.K.; Lv, X. Application of Biomass-Derived Nitrogen-Doped Carbon Aerogels in Electrocatalysis and Supercapacitors. *ChemElectroChem.* **2020**, *7*, 3695–3712.

27. Kumar, S.; Jena, A.; Hu, Y.C.; Liang, C.; Zhou, W.; Hung, T.F.; Chang, W.S.; Chang, H.; Liu, R.S. Cobalt Diselenide Nanorods Grafted on Graphitic Carbon Nitride: A Synergistic Catalyst for Oxygen Reactions in Rechargeable Li-O_2 Batteries. *ChemElectroChem.* **2018**, *5*, 29–35. [CrossRef]
28. Hei, Y.; Li, X.; Zhou, X.; Liu, J.; Sun, M.; Sha, T.; Xu, C.; Xue, W.; Bo, X.; Zhou, M. Electrochemical sensing platform based on kelp-derived hierarchical meso-macroporous carbons. *Anal. Chim. Acta* **2018**, *1003*, 16–25. [CrossRef]
29. Zhou, Y.; Tian, R.; Duan, H.; Wang, K.; Guo, Y.; Li, H.; Liu, H. CoSe/Co nanoparticles wrapped by in situ grown N-doped graphitic carbon nanosheets as anode material for advanced lithium ion batteries. *J. Power Sources.* **2018**, *399*, 223–230. [CrossRef]
30. Jiang, D.; Xu, Q.; Meng, S.; Xia, C.; Chen, M. Construction of cobalt sulfide/graphitic carbon nitride hybrid nanosheet composites for high performance supercapacitor electrodes. *J. Alloys Compd.* **2017**, *706*, 41–47. [CrossRef]
31. Hammer, B.; Nørskov, J. Electronic factors determining the reactivity of metal surfaces. *Surf. Sci.* **1995**, *343*, 211–220. [CrossRef]
32. Vayner, E.; Sidik, R.A.; Anderson, A.B.; Popov, B.N. Experimental and Theoretical Study of Cobalt Selenide as a Catalyst for O_2 Electroreduction. *J. Phys. Chem. C* **2007**, *111*, 10508–10513. [CrossRef]
33. Wang, X.; Zhuang, L.; He, T.; Jia, Y.; Zhang, L.; Yan, X.; Gao, M.; Du, A.; Zhu, Z.; Yao, X.; et al. Grafting Cobalt Diselenide on Defective Graphene for Enhanced Oxygen Evolution Reaction. *iScience.* **2018**, *7*, 145–153. [CrossRef] [PubMed]
34. Li, K.; Cheng, R.; Xue, Q.; Meng, P.; Zhao, T.; Jiang, M.; Guo, M.; Li, H.; Fu, C. In-situ construction of Co/CoSe Schottky heterojunction with interfacial electron redistribution to facilitate oxygen electrocatalysis bifunctionality for zinc-air batteries. *Chem. Eng. J.* **2022**, *450*, 137991. [CrossRef]
35. Harzandi, A.M.; Shadman, S.; Nissimagoudar, A.S.; Kim, D.Y.; Lim, H.D.; Lee, J.H.; Kim, M.G.; Jeong, H.Y.; Kim, Y.; Kim, K.S. Ruthenium Core–Shell Engineering with Nickel Single Atoms for Selective Oxygen Evolution via Nondestructive Mechanism. *Adv. Energy Mater.* **2021**, *11*, 2003448. [CrossRef]
36. Medford, A.J.; Moses, P.G.; Jacobsen, K.W.; Peterson, A.A. A Career in Catalysis: Jens Kehlet Nørskov. *ACS Catal.* **2022**, *12*, 9679–9689. [CrossRef]
37. Liu, P.; Yan, J.Y.; Mao, J.X.; Li, J.W.; Liang, D.X.; Song, W.B. In-plane intergrowth CoS_2/MoS_2 nanosheets: Binary metal–organic framework evolution and efficient alkaline HER electrocatalysis. *J. Mater. Chem. A* **2020**, *8*, 11435. [CrossRef]
38. Nørskov, J.K.; Rossmeisl, J.; Logadottir, A.; Lindqvist, L.; Kitchin, J.R.; Bligaard, T.; Jónsson, H. Origin of the Overpotential for Oxygen Reduction at a Fuel-Cell Cathode. *J. Phys. Chem. B* **2004**, *108*, 17886–17892. [CrossRef]

Disclaimer/Publisher's Note: The statements, opinions and data contained in all publications are solely those of the individual author(s) and contributor(s) and not of MDPI and/or the editor(s). MDPI and/or the editor(s) disclaim responsibility for any injury to people or property resulting from any ideas, methods, instructions or products referred to in the content.